Check for updates

Systematic spectral shifts in the mid-infrared spectroscopy of aerosols

LUKE MAIDMENT,[1,2,*] PETER G. SCHUNEMANN,[3] RHEA J. CLEWES,[2] MARTIN D. BOWDITCH,[2] CHRISTOPHER R. HOWLE,[2] AND DERRYCK T. REID[1]

[1]*Scottish Universities Physics Alliance (SUPA), Institute of Photonics and Quantum Sciences, School of Engineering and Physical Sciences, Heriot-Watt University, Edinburgh EH14 4AS, UK*
[2]*Defence Science and Technology Laboratory, Porton Down, Salisbury SP4 0JQ, UK*
[3]*BAE Systems, Inc., MER15-1813, P.O. Box 868, Nashua, NH, 03061-0868, USA*
[*]lm345@hw.ac.uk

Abstract: Infrared spectroscopy in the spectral fingerprint region from 6.5 to 20 µm has been applied for decades to identify vapor- and condensed-phase chemicals with high confidence. By employing a unique broadband laser operating from 7.2- to 11.5-µm we show that, in this region, wavelength-dependent Mie-scattering effects substantially modulate the underlying chemical absorption signature, undermining the ability of conventional infrared absorption spectroscopy to identify aerosolized liquids and solids. In the aerosol studied, Mie theory predicts that the positions of spectroscopic features will blue-shift by up to 200 nm, and this behavior is confirmed by experiment, illustrating the critical importance of considering Mie contributions to aerosol spectroscopy in the mid infrared. By examining the spectroscopy of light scattered from an aerosol of the chemical diethyl phthalate, we demonstrate excellent agreement with a Mie-scattering model informed by direct measurements of the particle-size-distribution and complex refractive index.

References and links

1. C. E. Kolb and D. R. Worsnop, "Chemistry and Composition of Atmospheric Aerosol Particles," Annu. Rev. Phys. Chem. **63**(1), 471–491 (2012).
2. C. F. Bohren and D. R. Huffman, *Absorption and Scattering of Light by Small Particles* (Wiley-VCH, 2004).
3. S. Arnold, M. Neuman, and A. B. Pluchino, "Molecular spectroscopy of a single aerosol particle," Opt. Lett. **9**(1), 4–6 (1984).
4. R. M. Sullenberger, S. M. Redmond, D. Crompton, A. M. Stolyarov, and W. D. Herzog, "Spatially-resolved individual particle spectroscopy using photothermal modulation of Mie scattering," Opt. Lett. **42**(2), 203–206 (2017).
5. A. Aiuppa, L. Fiorani, S. Santoro, S. Parracino, M. Nuvoli, G. Chiodini, C. Minopoli, and G. Tamburello, "New ground-based lidar enables volcanic CO_2 flux measurements," Sci. Rep. **5**(1), 13614 (2015).
6. R. E. H. Miles, A. E. Carruthers, and J. P. Reid, "Novel optical techniques for measurements of light extinction, scattering and absorption by single aerosol particles," Laser Photonics Rev. **5**(4), 534–552 (2011).
7. K. P. Gurton, M. Felton, R. Dahmani, and D. Ligon, "In situ infrared aerosol spectroscopy for a variety of nerve agent simulants using flow-through photoacoustics," Appl. Opt. **46**(25), 6323–6329 (2007).
8. K. B. Aptowicz, Y.-L. Pan, R. K. Chang, R. G. Pinnick, S. C. Hill, R. L. Tober, A. Goyal, T. Jeys, and B. V. Bronk, "Two-dimensional angular optical scattering patterns of microdroplets in the mid infrared with strong and weak absorption," Opt. Lett. **29**(17), 1965–1967 (2004).
9. L. Maidment, Z. Zhang, C. R. Howle, and D. T. Reid, "Stand-off identification of aerosols using mid-infrared backscattering Fourier-transform spectroscopy," Opt. Lett. **41**(10), 2266–2269 (2016).
10. L. Maidment, P. G. Schunemann, and D. T. Reid, "Molecular fingerprint-region spectroscopy from 5 to 12 µm using an orientation-patterned gallium phosphide optical parametric oscillator," Opt. Lett. **41**(18), 4261–4264 (2016).
11. S. L. Bartelt-Hunt, D. R. U. Knappe, and M. A. Barlaz, "A review of chemical warfare agent simulants for the study of environmental behavior," Crit. Rev. Environ. Sci. Technol. **38**(2), 112–136 (2008).

12. A. Kocak, S. L. Berets, V. Milosevic, and M. Milosevic, "Using the Kramers-Kronig method to determine optical constants and evaluating its suitability as a linear transform for near-normal front-surface reflectance spectra," Appl. Spectrosc. **60**(9), 1004–1007 (2006).
13. J. Schäfer, "MatScat," http://www.mathworks.com/matlabcentral/fileexchange/36831-matscat.
14. M. Kumar, M. N. Islam, F. L. Terry, Jr., M. J. Freeman, A. Chan, M. Neelakandan, and T. Manzur, "Stand-off detection of solid targets with diffuse reflection spectroscopy using a high-power mid-infrared supercontinuum source," Appl. Opt. **51**(15), 2794–2807 (2012).
15. M. T. Dohm, A. M. Potscavage, and R. F. Niedziela, "Infrared optical constants for carvone from the Mie inversion of aerosol extinction spectra," J. Phys. Chem. A **108**(25), 5365–5376 (2004).

1. Introduction

Aerosols are ensembles of small particles suspended in a gas. Understanding their behavior is important because of the role played by atmospheric aerosols in human health, the environment and climate change [1], as well as safety implications in industry from aerosols of hazardous chemicals and in a military context from chemical warfare agents (CWAs). The wavelength dependence of light scattered from an aerosol depends on many factors including the number and density of particles, the distribution of particle sizes, the complex refractive index of the material, the observation angle and the polarizations of the incident and scattered light fields. As illustrated later, these effects lead to significant wavelength shifts in the location of spectroscopic features, undermining the value of the archive spectra normally relied on for chemical identification, unless they are corrected appropriately.

The scattering and absorption of light by a dielectric sphere of arbitrary diameter is described by Mie theory [2]. Although developed early in the 20th century, the practical predictions of Mie theory could only be made—and as a consequence tested experimentally—once computers of sufficient power became available. Using a photo-thermal approach, Arnold, Neuman and Pluchino [3] measured the first absorption spectrum of a single aerosol particle in 1983, observing a clear feature between 7.8 – 10.3 µm from a 5.4-µm-diameter drop of ammonium sulphate ($(NH_4)_2SO_4$), consistent with both the absorption spectroscopy of $(NH_4)_2SO_4$ and Mie theory calculations. A modern implementation, using a tuneable quantum cascade laser instead of a globar as a mid-infrared source, measured the absorption of silica and PMMA microspheres while simultaneously imaging the spheres [4]. It is important to distinguish these measurements, in which the mid-infrared absorption of a single aerosol droplet is measured, from those in which the scattered light itself is recorded. The most well-established technique in which light scattered from an aerosol provides the measured signal is differential absorption LIDAR (DIAL), but here the aerosol (mainly atmospheric water droplets) serves primarily as a retroreflector to permit the path-integrated gas concentration to be measured at two wavelengths (e.g. CO_2 concentration [5],). By contrast, in this paper we describe what we believe to be the first broadband measurements of mid-infrared light scattered from an aerosol in which the interplay between bulk spectroscopic properties and wavelength-dependent scattering behavior is not only clearly observed but also explained by theory.

Most reported measurements of scattering from aerosol particles have been made at a single, visible or near-IR wavelength (a range of measurements is discussed in a review by Miles, Carruthers and Reid [6]). There are only a few examples in the published literature of measured mid-infrared optical properties. Gurton *et al*. attempted to characterize the mid-infrared optical properties of several chemical aerosols (as an ensemble of particles of different sizes, rather than a single particle), by measuring each aerosol's extinction cross section with Fourier-transform infrared (FTIR) spectroscopy from 3 – 13 µm, while simultaneously measuring the absorption cross-section using photoacoustic spectroscopy at several CO_2-laser wavelengths [7]. This technique was limited by the low resolution of the refractive index data used for the associated Mie theory calculations. There is only one example of a direct scattered light spectral measurement of single particles, at discrete wavelengths of 3.4 and 5.1 µm [8]. The scattering patterns from individual drops of both regular and heavy water were directly imaged at these wavelengths. Our prior work, examining the scattering from ensembles of two types of chemical aerosol between 3.2 – 3.55 µm [9], is the only report of a broad spectrum mid-infrared

scattering measurement to our knowledge. Here we extend these measurements deeper into the mid-infrared and, by comparing our results to a theoretical simulation, show that the scattered light spectrum is strongly influenced by Mie scattering.

2. Modelling and experiment

Figure 1(a) shows the layout of the experiment. The optical parametric oscillator (OPO, described in detail in [10]) produces a collimated mid-infrared beam, tunable by changing the grating period of the nonlinear medium. The scanning Michelson interferometer acts as a Fourier transform spectrometer. A HeNe laser monitors the scanning mirror displacement (driven by a voice-coil actuator), enabling the mid-infrared fringes to be calibrated onto an absolute distance scale, providing a stable and accurate wavelength scale after Fourier transforming the fringes. We verify the wavelength-scale calibration using a polystyrene reference card with independently calibrated absorption features.
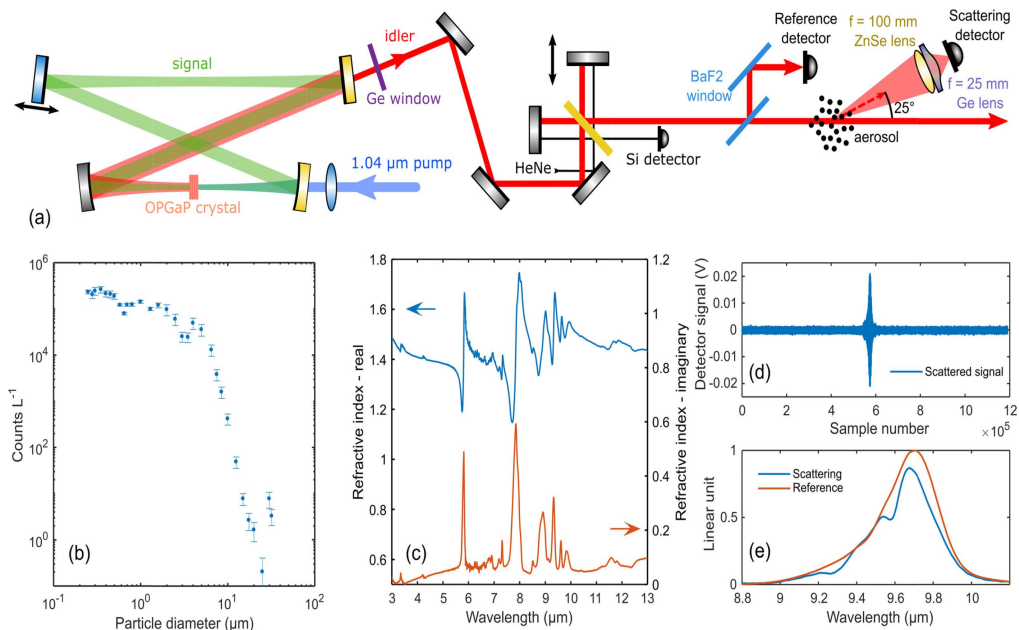

Fig. 1. (a) The mid-infrared idler beam from an orientation patterned gallium phosphide (OPGaP) OPO passes through a scanning Michelson interferometer acting as a Fourier transform spectrometer (using a ZnSe beamsplitter coated for $7 - 14$ µm). A weak reflection of the beam is measured on an HgCdTe detector to provide a reference spectrum. The main mid-infrared beam is directed through the aerosol, and scattered light is collected and focused onto the scattering detector. (b) Size distribution of aerosolized DEP. (c) Real (blue) and imaginary (orange) parts of the complex refractive index of DEP (d) Example of the data recorded during the experiment, showing an interferogram recorded on the scattered light detector. (e) Example of the measured spectra from the reference (orange) and scattered light (blue) detectors.

The chemical selected for this study was diethyl phthalate (DEP), an aromatic hydrocarbon (formula $C_{12}H_{14}O_4$, CAS number 84-66-2) which is liquid at room temperature and used as a CWA simulant [11]. An aerosol of DEP was produced by using a medical nebulizer, designed for creating aerosols of medicine for inhalation. The aerosol plume produced by the medical nebuliser was measured using a Grimm portable Laser Aerosol Spectrometer (Model Mini-LAS 11-R) which records particle size (between 0.25 and 32.00 µm over 31 channels) and number (1–2,000,000 particles L^{-1}). The measured particle-size distribution of aerosolized DEP is shown in Fig. 1(b) and comprised a range of particle diameters from 250 nm to 10 µm. The wavelength-dependent complex refractive index for DEP was recorded using a Bruker Tensor 37 FTIR spectrometer configured with a mid-infrared source, potassium bromide beamsplitter

and a DLaTGS detector. 1 mL of DEP was applied to a PTFE boat, inserted into a variable angle reflection accessory set at 0.5° from normal. The resultant reflectance spectra were converted into the real and imaginary refractive indices, shown in Fig. 1(c), using the Kramers-Kronig function [12].

Together, these data were applied to calculate the scattering cross-section into a particular solid angle using the following method. A spherical particle scatters incident p and s polarized electric fields according to [2]:

$$\begin{pmatrix} E_p \\ E_s \end{pmatrix} = \frac{e^{ik(r-z)}}{-ikr} \begin{pmatrix} S_2 & 0 \\ 0 & S_1 \end{pmatrix} \begin{pmatrix} E_{p_0} \\ E_{s_0} \end{pmatrix} \tag{1}$$

where k is the magnitude of the wave vector $\left(k = \frac{2\pi n_{real}}{\lambda} \right)$.

The S matrix components represent the sum of all the oscillating electric field dipoles. The matrix elements are calculated using the radius and complex refractive index of a particle using a Matlab code by Schäfer [13]. Considering a spherical polar coordinate system, S_1 and S_2 are dependent on θ and φ ($\theta = 0°$ is forward scattering, $\theta = 180°$ is backscattering). The scattered light intensity for a particular angle is:

$$\frac{I_{sca}}{I_0} = \frac{\left| S_j(\theta) \right|^2}{k^2 r^2} \tag{2}$$

with $j = 1$ for s polarization, and $j = 2$ for p polarization. I_0 is the incident intensity and r is the particle radius. This can be included in the expression for the differential cross-section (energy scattered per unit time into a unit solid angle):

$$\frac{dC_{sca}}{d\Omega} = \frac{\left| S_j(\theta) \right|^2}{k^2} \tag{3}$$

For spherical polar coordinates, $d\Omega = \sin\theta d\theta d\varphi$, so the scattering cross section can be found from the integral:

$$C_{sca} = \frac{1}{k^2} \int_{d\Omega} \left| S_j(\theta) \right|^2 \sin\theta d\theta d\varphi \tag{4}$$

By adding appropriate limits for θ and φ, this expression can be numerically integrated over a solid angle representative of the solid angle that the scattered light collection lens defines. The scattered power can be calculated simply by $P_{sca} = I_0 C_{sca}$.

The power scattered by an ensemble of particles can be calculated, relying on two assumptions which are summarized in [2] and [6] and require the particle density to be sufficiently sparse to prevent coupling of induced dipole moments between neighboring particles. The aerosols we generate fulfill this condition, so the scattered light by a particle distribution can be calculated by summing the contributions of individual particles:

$$P_{sca_{dist}} = \sum_{i=1}^{n} p_i P_{sca}(d_i) \tag{5}$$

where p_i is the number of particles of diameter d_i. In this way, the power scattered into a given solid angle for an aerosol of a particular size distribution and complex refractive index, and incident light of a certain polarization, can be calculated. By calculating this for many wavelengths, a scattered light spectrum can be found. The results of this simulation are

presented in Fig. 2(a) for wavelengths from 3 – 12 µm, for p polarization and for a forward scattering angle of 25°, which corresponded to the experimental geometry. For comparison, the transmission spectrum of liquid DEP is also shown, with the simulation results normalised to this. These data illustrate immediately the importance of measurements in the spectral fingerprint region: the richness, density and diagnostic potential of the spectral features are much greater in the 6.5 – 12 µm band than at shorter wavelengths. The effect of Mie-scattering on modifying the shapes and positions of bulk spectral features can be clearly seen, for example in the blue-shifting by up to 200 nm of the features near 8 µm and 9 µm.
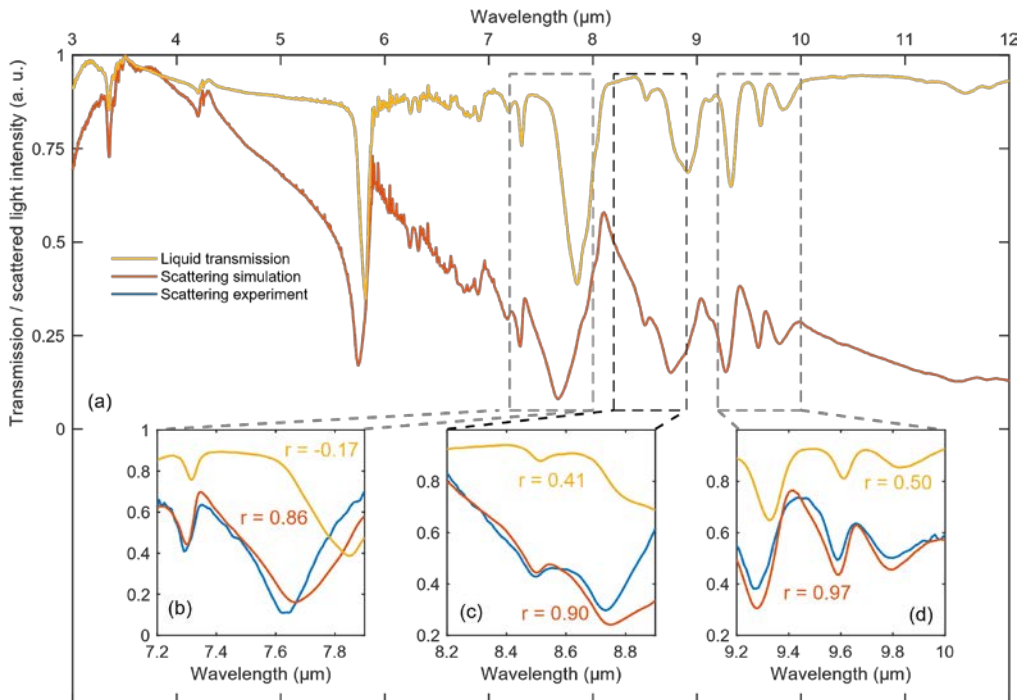

Fig. 2. (a) Mid-infrared liquid transmission spectrum for DEP (yellow) and the simulated scattered light spectrum for an aerosol of DEP with the measured size distribution and refractive index, for p-polarized incident light measuring at an angle of 25 degrees (orange). (b-d) Reproduction of the spectra in (a) over a narrower wavelength interval, with the experimentally measured scattered light spectrum (blue). Pearson correlation coefficients (r values) between the experimental results and the simulated scattering and transmission spectra are displayed.

We tested the predictions of the Mie scattering model by recording the intensity of the light before and after scattering by the aerosol. To make a reference spectrum measurement, the idler beam exiting the interferometer was transmitted through a wedged barium fluoride window at 45 degrees. We used two wedged window reflections to attenuate the power sufficiently to avoid saturation (and etalon effects that arise from other attenuation methods such as ND filters) of the liquid-nitrogen-cooled HgCdTe detector (Kolmar, sensitivity from 3 – 12 µm).

The beam passed 10 mm above the nebulizer output. Scattered light was collected by a ZnSe lens (focal length, 100 mm) at an angle of 25 degrees from the beam propagation direction, and focused onto a second HgCdTe detector by a Ge lens (focal length, 25 mm). An example of a scattered light interferogram is shown in Fig. 1(e). The detector experienced high-frequency noise with a magnitude of about 10 mV, so electronic band pass filtering was used to make the interferogram more easily visible. This has no influence on the spectral measurement. Interferograms were recorded from both detectors simultaneously (avoiding any wavelength drift issues) then Fourier transformed to obtain their spectra. The scattering detector spectrum was divided by the reference to show the spectrum of light scattered by the aerosol.

3. Results and discussion

In Fig. 2 we present data addressing the wavelength range from 7.2 – 10 µm in three separate measurements, corresponding to operating the OPGaP OPO on three different gratings ($\Lambda = 27$, 29 and 31 µm). All measurements were made at 19°C and were based on the average of seven individual spectra recorded at 1.2 cm^{-1} resolution with a 250-ms acquisition time. Figures 2(b-d) compares the experimentally measured scattering spectra with a Mie simulation (blue and orange lines), and contrasts both with the liquid transmission spectra for DEP (yellow line). Data in Fig. 2(b) (wavelengths 7.2 – 7.9 µm) show close agreement between the Mie-simulation and experiment, with clear differences being evident between these and the liquid transmission spectrum, whose two prominent absorption features are shifted to shorter wavelengths in the experimental and simulated aerosol spectra. Similar trends can be seen in the data recorded at longer wavelengths (8.2 – 8.9 µm and 9.2 – 10.0 µm) in Figs. 2(b) and (c).

The y-axis values in the measured scattered light spectra are arbitrary; the shape and location of spectral features is what we compare. In Figs. 2(b-d) the data are plotted with the same y-axis scale as (a), and the experimental results are plotted (blue) again with arbitrary y-axis scale to show qualitatively how the spectra compare. The Pearson correlation coefficient is used to quantify the correlation between the experimental results and the liquid transmission and simulated scattering (which has been used before in spectrum recognition [14], and provides a correlation measure which is insensitive to the intensity differences between the data sets). Clearly, the simulated scattering correlates much more strongly with the results, with values ≥ 0.86, while the transmission spectra values are ≤ 0.5.

DEP has no distinct spectral features beyond 10 µm, but we extended our study to wavelengths above 10 µm by using carvone, which is representative of chemicals which may be found in atmospheric aerosols [15] and has a spectral feature near 11 µm. Figure 3(a) shows the spectrum used to illuminate aerosolized carvone, and the spectrum of light scattered by it. The size distribution was not measured, so a simulated scattered light spectrum is not presented, but Fig. 3(b) clearly shows that the main spectral feature from the transmission spectrum of carvone is shifted to a lower wavelength in the aerosol scattering spectrum.
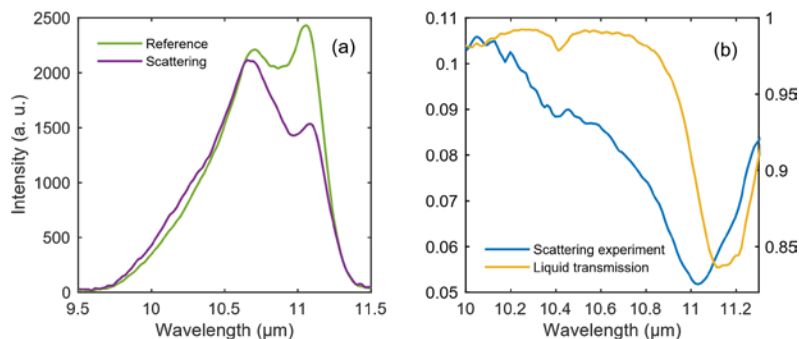

Fig. 3. (a) Spectra recorded on the reference (green) and scattering (purple) detectors for an aerosol of carvone. (b) Scattered light spectrum (blue) co-plotted with the transmission spectrum (yellow) of liquid carvone (calculated using data in [15]).

4. Conclusions

These results represent the first conclusive study showing how Mie scattering modulates the mid-infrared spectroscopic signature of aerosolized chemicals, with fundamental implications for interpretation of spectroscopic scattering data and for detection algorithm performance in scenarios as diverse as atmospheric modelling and stand-off chemical identification of hazardous agents. Understanding the spectral behavior of aerosols has been shown here to rely on adequate prior knowledge of the particle size distribution and the complex refractive index of the aerosolized chemical. The rapid development of coherent mid-infrared sources should

permit more routine aerosol scattering measurements in the spectral fingerprint region. We expect these to stimulate further investigations that examine scattering from a range of different particle size distributions, as well as studying solid aerosols (including non-spherical particles), some of which have implications for human health through their contribution to air pollution.

Funding